ISSN 1063-7842, Technical Physics, 2020, Vol. 65, No. 11, pp. 1709–1716. © Pleiades Publishing, Ltd., 2020.
Russian Text © The Author(s), 2020, published in Zhurnal Tekhnicheskoi Fiziki, 2020, Vol. 90, No. 11, pp. 1789–1796.

THEORETICAL AND MATHEMATICAL PHYSICS

Optimization of an Anode Membrane with a Transmission-Type Target in a System of Soft X-Ray Sources for X-Ray Nanolithography

P. Yu. Glagolev[a,*], G. D. Demin[a], G. I. Oreshkin[a], N. I. Chkhalo[b], and N. A. Djuzhev[a]

[a] *National Research University of Electronic Technologies, Moscow, 124498 Russia*

[b] *Institute for Physics of Microstructures, Russian Academy of Sciences, Nizhny Novgorod, 603950 Russia*

**e-mail: skirdovf@mail.ru*

Received April 16, 2020; revised April 16, 2020; accepted April 16, 2020

Abstract—In this paper, we propose a method for optimizing the design and composition of the anode membrane with a transmission-type target as part of a system of soft X-ray sources based on field-emission triodes for performing tasks in the field of X-ray nanolithography. It allows to prevent the degradation of the operating characteristics of the system when significant electrostatic deformation of the anode occurs under the influence of a control electric field in the inter-electrode space of the triodes. For this purpose, the inclusion of an additional control electrode in the system design is considered, which makes it possible to compensate for the deformation of the anode membrane to an acceptable level and thereby stabilize the operation of X-ray sources. A numerical model of the electrostatic deflection of the anode assembly in a modified design is developed, based on which the optimal composition and geometric parameters of the anode membrane with a compensating electrode are determined. In particular, the optimal distance between the anode membrane in the initial (undeformed) state and the compensating electrode was found (equal to 5 μm), at which a minimum voltage difference (about 1.15 kV) should be applied to these electrodes to prevent critical deflection of the membrane (0.72 μm with a membrane radius of 750 μm). It is also shown that, due to their extremely high hardness (>80 GPa), diamond-like films are the most promising material for the anode electrode. The results obtained can also be useful for the development of miniature X-ray generation devices for various applications.

DOI: 10.1134/S1063784220110122

INTRODUCTION

Currently, there is a rapid revival of one of the key areas of physics: field emission electronics, in which impressive results have been achieved over the past few years, both in the field of breakthrough experimental research [1–4] and in successful implementation of prototypes of solid-state electronic devices on its basis (diodes [5, 6], transistors [7, 8], nanosensors [9], portable X-ray tubes [10], etc.). Field emission electronics deals with the development of fundamental principles and technology for constructing electronic devices of the micro- and nanometer ranges, the principle of which is based on the effect of cold emission of electrons from a solid state medium into a vacuum (or quasi-vacuum) conducting channel under the influence of a strong electric field [11]. Since the ballistic transport of electrons in the vacuum channel occurs practically without collisions, vacuum electronics technology has a number of advantages over the semiconductor technology: vacuum micro- and nanoelectronic devices can operate at higher frequencies (in the sub-THz and THz regions), in a wider temperature range, and in the presence of strong radiation. At the same time, the operation of semiconductor devices under such extreme conditions is often unstable, which limits their use in the most important sectors of the economy (space research, nuclear energy, oil and gas production).

On the other hand, a relevant issue of modern nanoelectronics is to ensure the scaling of electronic components to the minimum design standards (up to 10 nm and below), which requires the use of new high-resolution lithographic methods [12]. One of these methods is maskless X-ray nanolithography using X-ray wavelengths in the range from 0.4 to 4 nm to form topological patterns with a limiting resolution in the range of tens of nanometers [13]. Unlike its competitors, the X-ray nanolithography process does not require the use of expensive masks, has a high speed and allows the formation of structures with a large aspect ratio (up to 100 : 1 [14]). These advantages can be achieved by using a system of miniature X-ray sources based on field-emission triode structures, which has low power consumption and is capable of

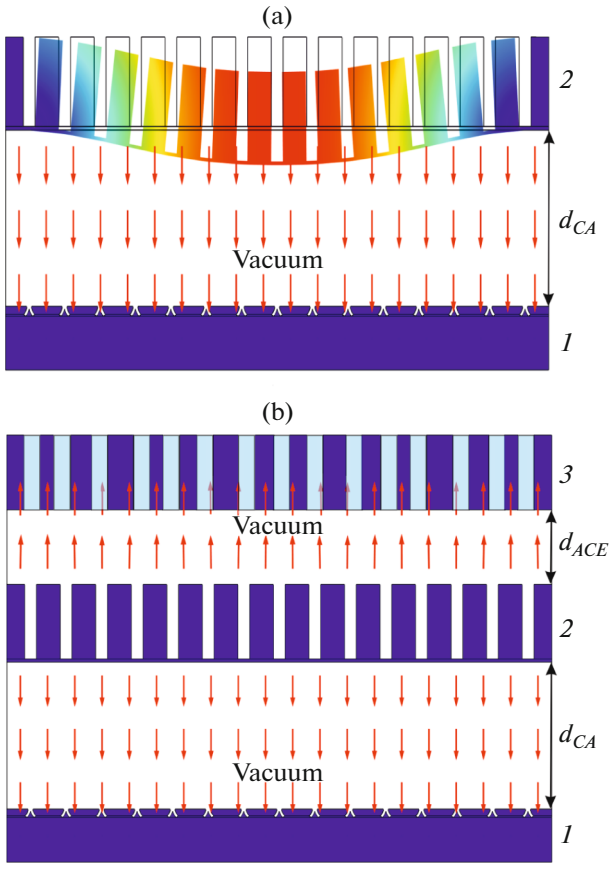

Fig. 1. Schematic representation of a system of soft X-ray radiation sources based on a matrix of field emission cathode nodes (FECN) and a matrix of anode nodes (a) without a compensating electrode and (b) with a compensating electrode. The FECN matrix (*1*) consists of a set of silicon needle-type cathodes with control grid electrodes. The matrix of anode nodes (*2*) in the initial design consists of a beryllium transmission-type target located on a perforated anode membrane. The compensating electrode (*3*) is designated for minimization of the electrostatic deflection of the matrix of anode nodes. Arrows indicate the direction of the electric field vector.

providing fast scanning (sequential passage of scan lines into which the generated topological pattern is divided) and maskless exposure of the sample to an X-ray beam for instant formation of a topological pattern on it [15]. A sample is a structure (e.g., a silicon wafer with a list of functional layers) obtained during technological operations (oxidation, deposition, sputtering, etc.) with an X-ray resist applied to it, from which individual topological elements will be formed using X-ray nanolithography. Such X-ray sources are extremely effective for other applications as well, such as medical technology, equipment for X-ray fluorescence analysis, security systems, etc.

Field-emission triode structures in X-ray sources make it possible to create a directed flux of high-energy electrons rapidly flying from the cathode to the anode with a transmission-type X-ray target (in less than 1 ps, a cathode–anode distance of several tens of microns [16]). In turn, the size of the electron beam is regulated under the action of the control voltage of the grid electrode, which ensures the production of focal spots of small diameter on the transmission-type-type target, which is necessary for the generation of narrowly directed electromagnetic waves in the X-ray range.

Earlier, in [17–19], we considered a conceptual and technological basis for creating an array of microfocus X-ray tubes based on an electronic system from a matrix of anode nodes (perforated anode membrane with a transmission-type target) and a matrix of field-emission cathode-grid nodes (FECNs) represented in the form of silicon needle-type cathodes with a set of control grid electrodes (Fig. 1a). In the process of modeling of the electronic system, it was revealed that, when a feed voltage applied to the anode is sufficient for the rise of a field-emission current, electrostatic deformation of the anode membrane occurs, which can adversely affect a wide range of key operating parameters of X-ray sources: the field emission current (lead to its fluctuations), the angular directivity of the X-ray radiation, and, as a consequence, the resolution of the topological pattern formed by the methods of maskless X-ray lithography [18]. To eliminate this negative effect, in this work, we propose a modification of the design of the matrix of anode nodes, which consists in adding an additional control electrode at a specified distance from the transmission-type target, the electric field from which compensates the deformation of the anode membrane (Fig. 1b). The solution proposed makes it possible to stabilize the operation of a system of soft X-ray radiation sources based on field emission triodes.

1. OPTIMIZING THE DESIGN OF THE MATRIX OF ANODE NODES

In the initial design, the system of microfocus X-ray tubes includes a matrix of FECNs, a matrix of anode nodes, and an X-ray optical MEMS mirror system [17]. A single FECN consists of a silicon nanocathode and the grid electrode line. The field emission current generated in the process of field emission of electrons from each element of the FECN matrix is controlled by the cut-off voltage on the corresponding buses of the grid electrodes. The matrix of anode nodes includes an X-ray-transparent beryllium film in which X-ray radiation is generated as a result of the action of an electron beam from the field-emission cathode on the film, and an anode membrane destined to create an electric field in the space between the anode node and the FECN. In the process of bonding the anode and cathode parts of the X-ray source system, the output X-ray windows of the matrix of the anode nodes are self-aligned with the cathode-grid nodes of the FECN matrix (located opposite each other), while its structure provides heat removal from the output trans-

mission-type target, which becomes critical during emission of high-energy electrons (over 1 keV). In this regard, it is an important task to choose the optimal composition and design of the matrix of anode nodes to ensure fast heat removal during the generation of X-ray radiation. Moreover, due to the strong electric fields required to generate field emission (on the order of several V/nm), the matrix of the anode nodes undergoes significant electrostatic deformation (Fig. 1a), which can significantly impede the stable operation of microfocus X-ray tubes as part of X-ray lithographer. An important factor affecting the directivity of the X-ray beam (radiation) is the spatial orientation of the X-ray windows in the anode matrix. Preliminary estimates show that maximum deflection $D_m^{\max}$ of the matrix of anode nodes, which determines the deviation of the X-ray windows from the vertical position in the deformed membrane, should not exceed the critical value $D_{M(\text{th})}^{\max}$ at which it becomes problematic to align the curvature of the image field on the plate with the X-ray resist by means of an optical MEMS mirror systems. The permissible curvature can be considered a value lying within $\pm D_{\text{of}} \approx \lambda/N_{\text{A}}^2$, where D_{of} is the focal depth of the projection lens and λ is the operating wavelength. In the object plane, this curvature corresponds to the maximum deviation $\Delta = \pm D_{\text{of}}M$, where M is the demagnification of the objective. For the model lithograph scheme, $N_{SA} = 0.4$, $\lambda = 11.4$ nm, $M = 10$ [18], and $D_{\text{of}} = 0.72$ μm. Hence, the permissible deviation $D_{M(\text{th})}^{\max}$ of the matrix of anode nodes from the plane is calculated, with is equal to ± 0.72 μm (the maximum range of height is about 1.42 μm) for the selected membrane diameter (1.5 mm).

To solve the above problems, in this work, we consider the optimization of the design of the matrix of anode nodes by introducing an additional control electrode at a given distance from the anode membrane, the electric field from which is capable of compensating its electrostatic deflection (Fig. 1b). To output X-ray radiation, the compensating electrode has X-ray windows of a larger diameter than in the perforated anode membrane, which is associated with the divergence of the X-ray beam after leaving the transmission-type target. To demonstrate the effectiveness of the proposed concept, we carried out a numerical simulation of the structure of the matrix of anode nodes with a compensating electrode in order to determine its optimal parameters.

2. MODEL OF ELECTROSTATIC DEFORMATION OF THE MATRIX OF ANODE NODES

In the COMSOL MultiPhysics software package [20], based on the finite element method, a model of electrostatic deformation of the matrix of anode nodes was constructed both with and without a compensating electrode in its structure (Fig. 1). This software package was chosen due to the presence in it of physical modules necessary for the simultaneous simulation of two interconnected physical processes: 1) the electric field distribution in the interelectrode space ("Electrostatics" module) and 2) mechanical deformation of the anode membrane under the action of the calculated electrostatic force arising between the matrix of anode nodes and the FECN matrix ("Solid Mechanics" module). For the correct presentation of the results, the option of the Laplace smoothing of the computational grid during its construction was provided for the case of a deformable shape of the matrix of anode nodes.

3. BASIC EQUATIONS

Electrostatic field $\mathbf{E} = -\nabla V$ in the vacuum space between the matrix of the anode nodes and the FECN matrix is calculated from the numerical solution of Poisson's equation represented in a differential form,

$$-\nabla(\varepsilon_m \nabla V) = \frac{\rho_V^m}{\varepsilon_0}, \tag{1}$$

where ε_0 is the permittivity of vacuum, ε_m is the permittivity of the medium, and ρ_V^m is the volume charge density in the mth medium. In vacuum, it is assumed that $\rho_V^{\text{vac}} = 0$ and $\varepsilon_m = 1$.

The initial conditions are potential $V = V_A$ at the matrix of anode nodes and the zero potential ($V = 0$) at the FECN matrix (in the approximation that the voltage at the grid electrode (on the order of several tens of volts) does not have a strong effect on the deformation of the anode membrane).

The magnitude of the field $\mathbf{E} = \mathbf{E}_A$ at the anode membrane surface is necessary for calculating vector $\mathbf{u}$ of the deformation of the matrix of anode nodes under the action of electrostatic force $\mathbf{f}_e$, which corresponds to the equation

$$\nabla(FS)^T + \mathbf{F}_{gV} = 0, \tag{2}$$

where $F = \nabla\mathbf{u} + I$, I is the unit tensor, and $\mathbf{F}_{gV}$ is the external gravitational force acting on the unit volume of the anode membrane. It should be noted that the force of gravity has no noticeable effect on the deflection of the membrane under the action of an electrostatic force in the interelectrode space. Therefore, the value of $\mathbf{F}_{gV}$ in the calculations of the deformation of the matrix of the anode nodes can be neglected. The second Piola–Kirchhoff stress tensor is determined by the formula

$$S = 2\frac{\partial H_{\text{eme}}}{\partial C}, \tag{3}$$

where $C = F^T F$ is the fourth-rank elastic tensor and electric enthalpy H_{eme} (thermodynamic potential) neglecting the electric polarization of dielectrics

and the effect of electrostriction of materials is expressed as

$$H_{\text{eme}} = W_S(C) - 0.5\varepsilon_0 JC^{-1} : (\mathbf{E}_A \otimes \mathbf{E}_A), \quad (4)$$

where $J = \det(F)$, $W_S(C) = 0.5\varepsilon_{\text{el}} : (C : \varepsilon_{\text{el}} + 2\sigma_0) = 0.5\varepsilon_{\text{el}} : (\sigma + \sigma_0)$ is the elastic strain energy density (for the case of linear elastic materials), $\varepsilon_{\text{el}} = \varepsilon - = \varepsilon_{\text{inel}}$, ε is the general strain tensor of the material, $\varepsilon_{\text{inel}}$ is the inelastic strain tensor, σ is the electromechanical stress tensor, and σ_0 is the initial or external electromechanical stress tensor. To simplify the form of the above relationships, the operator ":" denotes a double tensor product.

We will also assume that the stress tensor is continuous at the interface between materials (boundary conditions):

$$\mathbf{n}_i(\sigma_{i+1} - \sigma_i) = 0, \quad (5)$$

where $\mathbf{n}_i$ is the vector normal to the boundary of the ith material and $\sigma_{i(i+1)}$ is the stress tensor in the $i(i+1)$th material. In a vacuum space (in the absence of magnetic fields), this tensor is described as $\sigma_{\text{vac}} = \varepsilon_0 \mathbf{E} \otimes \mathbf{E} - 0.5(\varepsilon_0 \mathbf{E} \cdot \mathbf{E})I$ and $(\mathbf{E} \otimes \mathbf{E})_{ij} = E_i E_j$.

In turn, to estimate electric field amplification coefficient β_C (the ratio of the maximum electric field strength on the cathode surface to the field strength between plane electrodes) at a needle-type cathode, we used an expression of the form

$$\beta_C = E_C^{\max} \frac{d_{CA}}{V_A}, \quad (6)$$

where $E_C^{\max}$ is the maximum field on the cathode surface (local electric field at its top) and d_{CA} is the distance between the FECN matrix and the matrix of anode nodes in the undeformed state (Fig. 1). This coefficient enables one to assess degree of change in the electric field $E_C^{\max}$ at the top of the cathode with distance d_{CA}, which is important for estimating the variation in the field emission current from each FECN element at a given electrostatic deflection of the membrane.

4. SIMULATION RESULTS

The simulation we performed makes it possible to determine the optimal physical and design parameters of the matrix of anode nodes with a compensating electrode, the inclusion of which is necessary to eliminate unwanted deformation of the anode membrane with a transmission-type target in the process of field emission. Carbon (diamond) was chosen as the material of the anode membrane, and the diameter of the membrane in the matrix of the anode nodes was taken equal to 1.5 mm. It should be noted that, during the simulation, the thickness of an anode node ($h_A = 10$ μm) and the thickness of the compensating electrode ($h_{CE} = 50$ μm) remained unchanged, while the anode voltage was initially fixed at a level of $C_A = 2$ kV, which is sufficient to maintain a stable field emission current. The variable geometric parameters were the following quantities: distance d_{CA} between the FECN matrix and the matrix of anode nodes in the initial (undeformed) state of the anode membrane and distance D_{ACE} between the anode membrane and the compensating electrode in the initial (undeformed) state of the anode membrane (Fig. 1).

Figure 2a shows the dependence of electric field amplification coefficient β_C at the tip of the cathode on distance d_{CA} between the FECN matrix and the undeformed matrix of anode nodes. As can be seen from the figure, this dependence is nonlinear, which is associated with a nonlinear decrease in maximum field $E_C^{\max}$ with increasing d_{CA}, which it is easy to see from Fig. 2b. In turn, according to formula (5), coefficient β_C smoothly increases in the range from 43.1 to 46.5 as the distance varies from 3 to 20 μm. Figure 2b shows that field $E_C^{\max}$ increases almost linearly with an increase in operating anode voltage V_A (from 1 to 2 kV) at large distances (10 and 20 μm), while, as the matrix of anode nodes approaches a needle-type cathode in the high-voltage region, a small nonlinear section of the dependence appears. In a given range of electric fields, stable field emission of electrons must be observed (the maximum value of field $E_C^{\max}$ on the surface of a silicon nanocathode exceeds threshold field-emission field E_{th}^{FE} of about 2 V/nm [21]). We also estimated the electrostatic deformation of the matrix of anode nodes in the absence of a compensating electrode. Figure 2c shows electrostatic deflection D_M of the anode membrane along radial line L_M on its surface at an anode voltage of 2 kV. This deflection noticeably exceeds the permissible deformation limit $D_{M(\text{th})}^{\max}$ equal to 0.72 μm for a given membrane diameter (1.5 mm), at which there is no change in the angular directivity of X-ray radiation and distortion of the resolution of the X-ray nanolithograph in the operating voltage range. The maximum electrostatic deformation $D_M^{\max}$ of the matrix of anode nodes in this case increases almost linearly with the voltage V_A, which follows from Fig. 2d. It should be noted that the distance d_{CA} was varied from 10 to 20 μm. The inclusion of a compensating electrode with control voltage V_{CE} in the structure of the matrix of anode nodes leads to a noticeable decrease in its deformation (by several times), which can be seen from the picture of the three-dimensional distribution of deformations over the surface of the anode membrane shown in Fig. 3. This figure corresponds to the case in which the voltage difference between the compensating electrode and the anode membrane is $V_{CE} - V_A = 2$ kV, distance $D_{CA} = 10$ μm, and $d_{ACE} = 10$ μm. Figure 4a shows the maximum electrostatic deformation of the anode

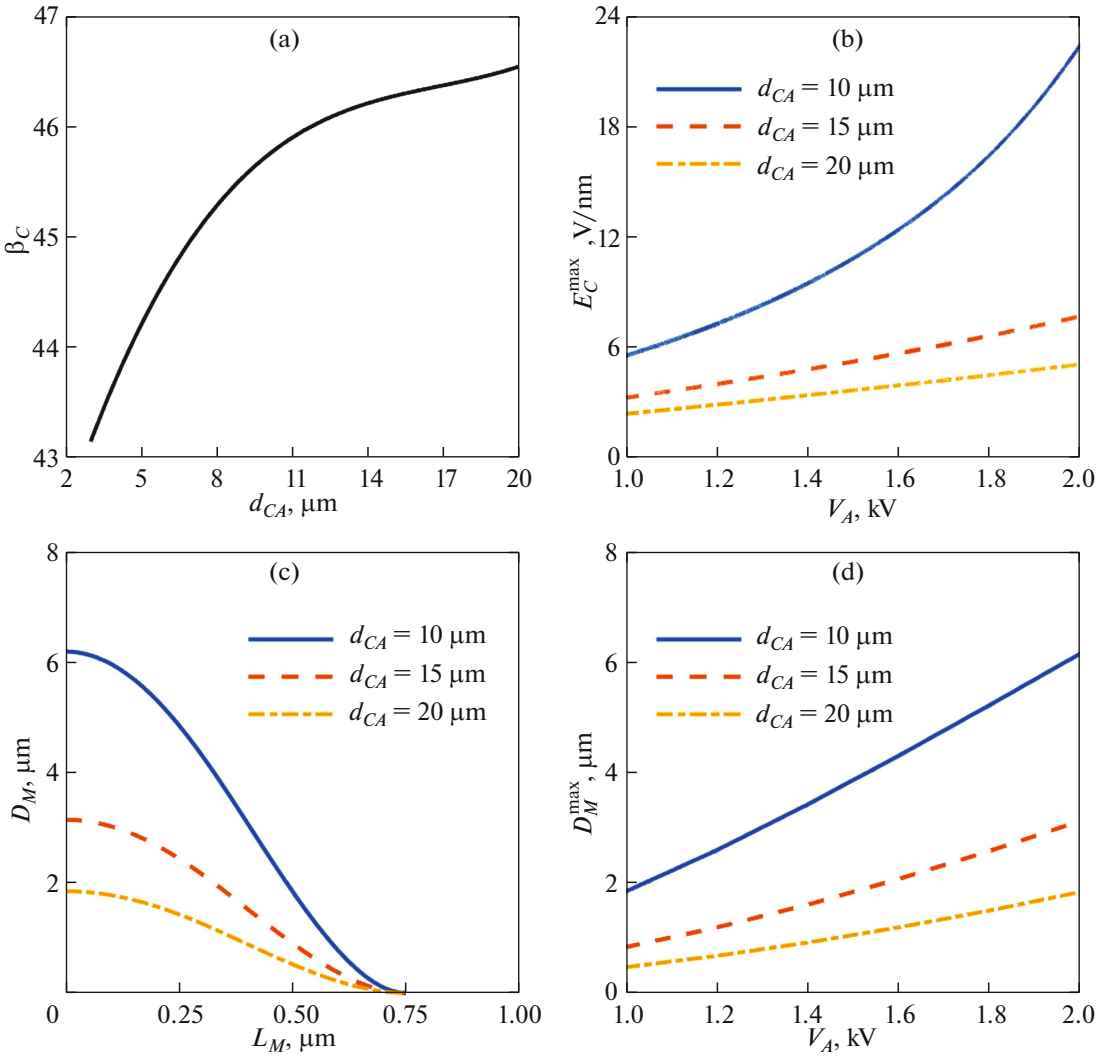

Fig. 2. (a) Amplification factor β_C of the electric field at the tip of the needle-type cathode vs. the distance between the FECN matrix and the matrix of anode nodes, d_{CA}; the anode voltage is $V_A = 2$ kV. (b) Maximum amplitude of the electric field, E_C^{max} at the tip of the needle-type cathode vs. voltage V_A at the anode membrane with different d_{CA}. (c) Electrostatic deflection of the anode membrane D_M along line L_M for various distances d_{CA} (at a voltage $V_A = 2$ kV), where the line L_M is the radial line going from the center of the membrane to its edge. (d) Maximum displacement D_M^{max} of the anode membrane vs. voltage V_A across the anode membrane for various d_{CA}.

membrane, D_M^{max}, in the presence of a compensating electrode as a function of the difference between the voltage at the compensating electrode, V_{CE}, and at the matrix of anode nodes, V_A, for different distances d_{ACE} (from 5 to 10 μm). The minimum (close to zero) deformation of the matrix of anode nodes was observed in the case of threshold values $(V_{CE} - V_A)_{th}$ equal to 1.15, 1.65, and 2.25 kV for corresponding distances d_{ACE} of 5, 7.5, and 10 μm. If $V_{CE} - V_A > (V_{CE} - V_A)_{th}$, the matrix of anode nodes is deformed in the opposite direction: toward the compensating electrode. Due to this feature, the curves in Fig. 4a are limited by the thin dashed line, the intersection with which corresponds to the case in which the deflection of the matrix of anode nodes is 70% of distance d_{ACE}. This boundary is taken with a margin and corresponds to the electric field E_{ACE}^{max} in the space between the anode and the compensating electrode, which is equal to 1 V/nm, i.e., 50% of threshold field E_{th}^{FE} at which the emission of electrons from the anode surface to the compensating electrode can begin and an unwanted contact and sticking of electrodes due to electrostatic forces is also possible. In this case, there is a linear dependence between the interelectrode distance d_{ACE} and the threshold voltage difference $(V_{CE} - V_A)_{th}$, at

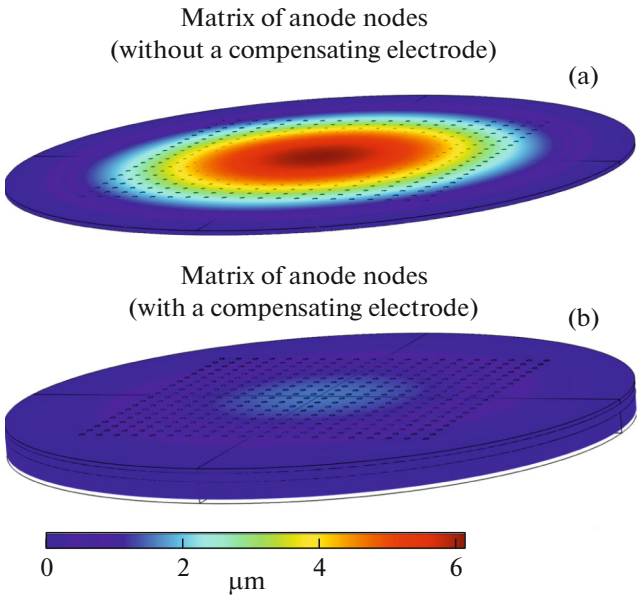

Fig. 3. Three-dimensional distribution of electrostatic deformation of the matrix of anode nodes (a) in the absence and (b) in the presence of a compensating electrode for $V_{CE} - V_A = 2$ kV, $d_{CA} = 10$ μm, and $d_{ACE} = 10$ μm.

which the deformation of the matrix of anode nodes is minimal (Fig. 4b). It should be noted that, at these values of $(V_{CE} - V_A)_{\text{th}}$, a field exceeding E_{th}^{FE}, at which an undesirable effect of electron emission in the space between the anode membrane and the compensating electrode may occur, is not achieved.

The variation of maximum $D_M^{\max}$ of electrostatic deformation of the matrix of anode nodes was also investigated for various materials of the anode membrane and compensating electrode at fixed distance $d_{ACE} = 5$ μm. This analysis was conducted in order to find the optimal composition of the anode matrix, making it possible to ensure the stable operation of the microfocus X-ray source even in the event of random deviations of the voltage difference $V_{CE} - V_A$ from its threshold value $(V_{CE} - V_A)_{\text{th}}$ at which the membrane deformation becomes minimum. As the material for the anode membrane and the compensating electrode, silicon (Si), aluminum (Al), and diamond-like (C) films were considered. Figure 5 shows the corresponding dependences of $D_M^{\max}$ on the voltage difference across the electrodes for these materials. As can be

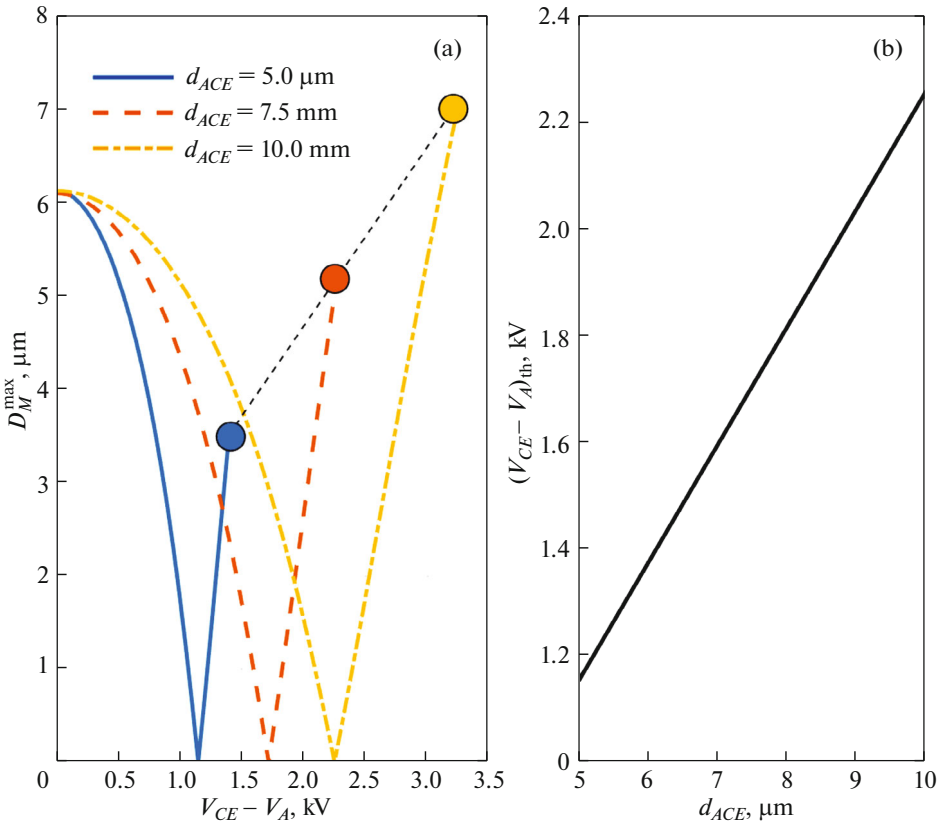

Fig. 4. (a) Maximum electrostatic deflection $D_M^{\max}$ of the matrix of anode nodes vs. voltage $V_{CE} - V_A$ for various distances d_{ACE} between the compensating electrode and the anode membrane. At the intersection of the curves with a thin dashed line, the deflection of the matrix towards the compensating electrode is 70% of distance d_{ACE} (round dots). (b) The threshold value of the voltage difference $(V_{CE} - V_A)_{\text{th}}$ between the compensating electrode and the anode membrane, at which the electrostatic deflection of the matrix of anode nodes is close to zero, vs. distance d_{ACE}. Distance d_{CA} in both cases is assumed to be 10 μm.

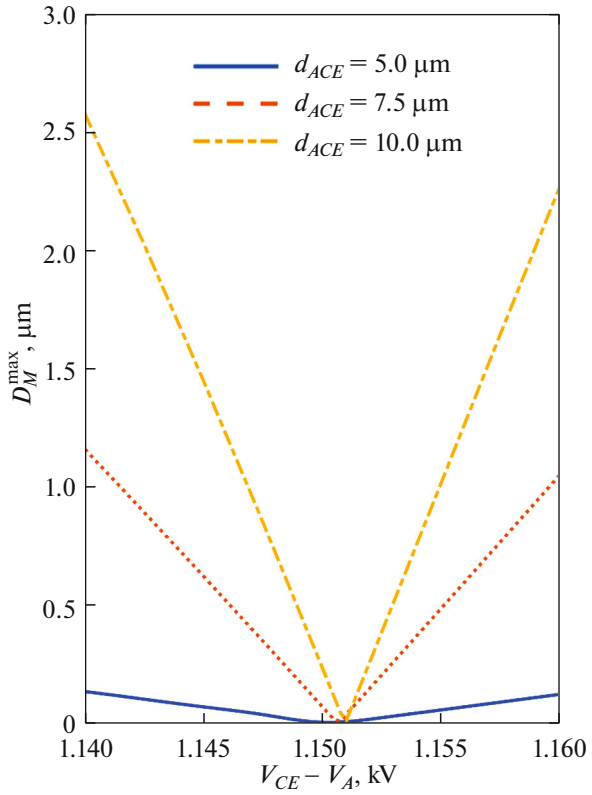

Fig. 5. Comparison of maximum electrostatic deflection D_M^{max} of the matrix of anode nodes (with a compensating electrode) for various anode membrane materials vs. the voltage difference between compensating electrode V_{CE} and anode membrane V_A. Distance d_{ACE} (anode membrane–compensating electrode) is 5 μm, and distance d_{CA} (FECN matrix–matrix of anode nodes) is 10 μm. Voltage V_A is assumed to be 2 kV.

seen from the figure, aluminum and silicon demonstrate the greatest steepness of the increase in deformation in the range of voltages from 1.14 to 1.16 kV (near the threshold value of 1.15 kV), which, ultimately, can lead to distortion of the directivity of X-ray radiation, as well as variations in the emission current in the space between the FECN matrix and the matrix of anode nodes. For this reason, diamond-like films with a stiffness higher than 80 GPa [22] and a smaller (compared to the materials we considered) variation in the deflection when the voltage difference $V_{CE} - V_A$ deviates from its threshold value $(V_{CE} - V_A)_{th}$ seem to be the most attractive for preventing random electrostatic deformation of the matrix of anode nodes. It should also be noted that diamond has a high thermal conductivity (in the range from 2000 to 2500 W/(m K) at a temperature of 300 K [23]), which prevents strong heating of the matrix of anode nodes by the field emission current and, thereby, increases the service life of an anode membrane based on diamond-like films.

CONCLUSIONS

Thus, have considered one of the ways to optimize the matrix of anode nodes in the composition of a microfocus X-ray source in order to minimize its electrostatic deformation during the flow of field emission current. For this purpose, we proposed to introduce into the matrix an additional control electrode at a given distance from the surface of the anode membrane, which opens up opportunities of adjusting and compensating its electrostatic deflection. Silicon, aluminum, and diamond-like films were considered as materials for the compensating electrode and the anode membrane. It follows from the simulation that the most suitable material for these electrodes is diamond-like films, since, in comparison with other materials, they are less susceptible to electrostatic deflection due to their extremely high stiffness (more than 80 GPa [22]). For this reason, electrodes made of this material exhibit resistance to deviation of the voltage difference $V_{CE} - V_A$ between the compensating electrode and the matrix of anode nodes from the threshold value $(V_{CE} - V_A)_{th}$, at which the deformation of the matrix is minimal. For the given interelectrode distances d_{ACE} varying in the range from 5 to 10 μm, the set of values of $(V_{CE} - V_A)_{th}$ has been determined. The chosen range of distances is optimal, since, in the case of $d_{ACE} < 5$ μm, a random voltage fluctuation near the threshold value $(V_{CE} - V_A)_{th}$ may cause sticking of the electrodes and, at distance $d_{ACE} > 10$ μm, the compensating electrode should be supplied with a voltage higher than 4 kV, which leads to strong heating of the anode membrane. A linear dependence has been found between the threshold voltage difference $(V_{CE} - V_A)_{th}$ and distance d_{ACE} between the anode membrane and the compensating electrode. This dependence implies that the minimum voltage difference $(V_{CE} - V_A)_{th} = 1.15$ kV is achieved at optimal distance $d_{ACE} = 5$ μm (when the interelectrode distance is $d_{ACE} = 10$ μm). The results obtained greatly facilitate the solution of the problem of the occurring electrostatic deflection of the matrix of anode nodes in soft X-ray radiation sources, which contributes to the stability and reliability of X-ray nanolithography processes based on them.

FUNDING

This work was supported by Russian Federation Presidential Council for Grants (grant no. 075-15-2019-1139) and carried out using the equipment of MIET Core facilities center "MEMS and electronic components" supported by the Ministry of Education and Science of the Russian Federation.

CONFLICT OF INTEREST

The authors declare that they have no conflicts of interest.

REFERENCES

1. J.-W. Han, M.-L. Seol, D.-I. Moon, G. Hunter, and M. Meyyappan, Nat. Electron. **2**, 405 (2019). https://doi.org/10.1038/s41928-019-0289-z
2. M. Liu, T. Li, and Y. Wang, J. Vac. Sci. Technol., B **35**, 031801 (2017). https://doi.org/10.1116/1.4979049
3. Y. Huang, Z. Deng, W. Wang, C. Liang, J. She, S. Deng, and N. Xu, Sci. Rep. **5**, 10631 (2015). https://doi.org/10.1038/srep10631
4. S. A. Guerrera and A. I. Akinwande, Nanotechnology **27**, 295302 (2016). https://doi.org/10.1088/0957-4484/27/29/295302
5. P. Zhang and Y. Y. Lau, J. Plasma Phys. **82** (5), 595820505 (2016). https://doi.org/10.1017/S002237781600091X
6. W.-T. Chang, H.-J. Hsu, and P.-H. Pao, Micromachines **10**, 858 (2019). https://doi.org/10.3390/mi10120858
7. J.-W. Han, D.-I. Moon, and M. Meyyappan, Nano Lett. **17**, 2146 (2017). https://doi.org/10.1021/acs.nanolett.6b04363
8. J. Xu, Z. Gu, W. Yang, Q. Wang, and X. Zhang, Nanoscale Res. Lett. **13**, 311 (2018). https://doi.org/10.1186/s11671-018-2736-6
9. M. Liu, Y. Lei, Y. Yang, T. Li, and Y. Wang, *Proc. Int. Conf. Manipulation, Automation and Robotics at Small Scales* (Helsinki, Finland, 2019), Vol. 1. https://doi.org/10.1109/marss.2019.8860991
10. N. A. Djuzhev, G. D. Demin, T. A. Gryazneva, V. Yu. Kireev, and D. V. Novikov, *IEEE Conf. of Russian Young Researchers in Electrical and Electronic Engineering (EIConRus)* (Moscow, Russia, 2018), p. 1974. https://doi.org/10.1109/EIConRus.2018.8317498
11. N. Egorov and E. Sheshin, *Field Emission Electronics* (Springer, 2017), Vol. 60. https://doi.org/10.1007/978-3-319-56561-3
12. E. M. Sebastian, S. K. Jain, R. Purohit, S. K. Dhakad, and R. S. Rana, Mater. Today (in press). https://doi.org/10.1016/j.matpr.2020.02.505
13. N. I. Chkhalo, A. Ya. Lopatin, A. E. Pestov, N. N. Salashchenko, G. D. Demin, N. A. Dyuzhev, and M. A. Makhiboroda, Proc. SPIE **11022**, 110221M (2018). https://doi.org/10.1117/12.2522105
14. C. Xue, J. Zhao, Y. Wu, H. Yu, S. Yang, L. Wang, W. Zhao, Q. Wu, Z. Zhu, B. Liu, X. Zhang, W. Zhou, and R. Tai, Appl. Surf. Sci. **425**, 553 (2017). https://doi.org/10.1016/j.apsusc.2017.07.010
15. N. A. Djuzhev, G. D. Demin, T. A. Gryazneva, A. E. Pestov, N. N. Salashchenko, N. I. Chkhalo, and F. A. Pudonin, Bull. Lebedev Phys. Inst. **45** (1), 1 (2018). https://doi.org/10.3103/S1068335618010013
16. N. I. Tatarenko and V. F. Kravchenko, *Autoemission Nanostructures and Devices Based on Them* (Fizmatlit, Moscow, 2006) [in Russion].
17. N. A. Djuzhev, G. D. Demin, N. A. Filippov, I. D. Evsikov, P. Y. Glagolev, M. A. Makhiboroda, N. I. Chkhalo, N. N. Salashchenko, S. V. Filippov, A. G. Kolosko, E. O. Popov, and V. A. Bespalov, Tech. Phys. **64** (12), 1742 (2019). https://doi.org/10.1134/S1063784219120053
18. N. N. Salashchenko, N. I. Chkhalo, and N. A. Djuzhev, J. Surf. Invest.: X-Ray, Synchrotron Neutron Tech. **12**, 944 (2018). https://doi.org/10.1134/S1027451018050324
19. G. D. Demin, N. A. Djuzhev, N. A. Filippov, P. Yu. Glagolev, I. D. Evsikov, and N. N. Patyukov, J. Vac. Sci. Technol., B **37**, 022903 (2019). https://doi.org/10.1116/1.5068688
20. *COMSOL Multiphysics v. 5.5, COMSOL AB (Stockholm, Sweden)*, https://www.comsol.com/
21. M. Ding, G. Sha, and A. I. Akinwande, IEEE Trans. Electron Devices **49**, 2333 (2002). https://doi.org/10.1109/TED.2002.805230
22. R. Hatada, S. Flege, M. N. Ashraf, A. Timmermann, C. Schmid, and W. Ensinger, Coatings **10**, 360 (2020). https://doi.org/10.3390/coatings10040360
23. S. L. Shinde and J. Goela, *High Thermal Conductivity Materials* (Springer, 2006). ISBN: 9780387251004

Translated by E. Chernokozhin